Contents lists available at ScienceDirect

European Journal of Mechanics / A Solids

journal homepage: www.elsevier.com/locate/ejmsol

Indentation of a free beam resting on an elastic substrate with an internal lengthscale

E. Radi [a,b,*], A. Nobili [b,c], M.A. Guler [d]

[a] Dipartimento di Scienze e Metodi dell'Ingegneria, Università di Modena e Reggio Emilia, 42122, Reggio Emilia, Italy
[b] Centro Interdipartimentale En&tech, Università di Modena e Reggio Emilia, 42122, Reggio Emilia, Italy
[c] Dipartimento di Ingegneria "Enzo Ferrari", Università di Modena e Reggio Emilia, 41125, Modena, Italy
[d] College of Engineering and Technology, American University of the Middle East, Kuwait

ARTICLE INFO

Keywords:
Unilateral contact
Couple stress elasticity
Euler-Bernoulli beam
Cubic eigenvalue problem
Size effect

ABSTRACT

The plane strain problem of a slender and weightless beam-plate loaded by a transversal point force in unilateral contact with a couple stress elastic foundation is investigated. The study aims to explore the consequences of the material internal lengthscale on the contact mechanics. In particular, compatibility between the beam and the foundation surface demands that both displacement and rotation match along the contact line. To this aim, couple tractions are exchanged besides the traditional contact pressure until separation between the beam and the foundation occurs. The problem is formulated making use of the Green's functions for a point force and a point couple acting atop of a couple stress elastic half-plane. A pair of coupled integral equations is thus derived, that governs the distribution of contact pressure and couple tractions, with one of them being immediately solved to provide an explicit relation between the two unknowns. In this sense, we retrieve the concept of a mechanically equivalent action, as it is the case of the Kirchhoff shear for plates. The remaining integral equation sets a cubic eigenvalue problem, whose linear term accounts for the microstructure. Its numerical solution is sought by expanding the equivalent contact pressure in series of Chebyshev polynomials vanishing at the contact region ends points, namely the lift-off points, and then applying a collocation strategy. The contact length, the distributions of contact pressure and couple tractions under the beam and the shearing force and bending moment along the beam are then obtained as a function of the material characteristic length. Results clearly indicate that accounting for the material internal lengthscale is mainly realized through exchange of the couple tractions, in the lack of which results much resemble those of the classical solution. Specifically, greater contact lengths and a stronger focusing effect about the loading point are encountered, which become very significant when the contact length approaches the internal lengthscale.

1. Introduction

Assessing mechanical contact of an elastic beam unilaterally supported by an elastic substrate endowed with an internal lengthscale (as it occurs, for instance, in the presence of material microstructure) is a fundamental endeavor in many scientific areas and lays the ground for several important applications. Indeed, it is a relevant issue for the railway industry, where it provides precious knowledge to detect damage on railway tracks (Yang et al., 2020), for biomedical applications such as implant design (Ghavidelnia et al., 2021) and bone reconstruction (Ermeyev et al., 2016a,b 2017) and in civil engineering, whose prototype problem is the design of beam foundations resting on granular materials. This classical problem is experiencing a renaissance in light of its applications in the growing sector of electronic sensing and actuation devices, specifically in the raising area of micro- and nano-electromechanical systems (MEMS/NEMS). Recently, MEMS/NEMS have raised a lot of attention in connection to modern advanced manufacturing technologies, such as additive printing. For how classical this problem may be, featuring a long history of models and applications, it is the lengthscale involved in the system that brings new challenges. It is well known that, at this micro/nano scale, the material's constitutive relations are different than those at the macro scale. To define such constitutive relations one of the most common material characterization tests used by the experimentalist is the indentation test

* Corresponding author. Dipartimento di Scienze e Metodi dell'Ingegneria, Università di Modena e Reggio Emilia, 42122, Reggio Emilia, Italy.
E-mail address: eradi@unimore.it (E. Radi).

https://doi.org/10.1016/j.euromechsol.2022.104804
Received 1 July 2022; Received in revised form 9 September 2022; Accepted 10 September 2022

at the macro level. It is also used at the micro-nano level to define the material behavior (Ma and Clarke, 1995; Briscoe et al., 1998; Elmustafa and Stone, 2002). When indentation tests are conducted at the nano scale, they give results that depend on the size of the indenter, hence the influence of size whose role becomes fundamental, especially if the contact size is comparable to the material lengthscale. Moreover, from the failure and reliability standpoint of the moving parts in MEMS/NEMS structures, controlling the stress state at the ends of the contact zone is of paramount importance in order to rule out the possibility of crack formation and catastrophic debonding.

The contact behavior of materials can be well investigated within the continuum theory of classical elasticity at the macro level. However, when size becomes a relevant issue, such it occurs at micro-nano level, the classical continuum theory fails for it is inherently self-similar, namely its structure is independent of the scale of the system under investigation. For this reason, enhanced constitutive theories have been proposed that introduce a length scale related to the material microstructure, thus spawning the broad class of complex media (Eringen, 1968, 1972, 1983; Lam et al., 2003; Mindlin and Tiersten, 1962; Toupin, 1962; Koiter, 1964; Gurtin et al., 1998; Jasiuk and Ostoja-Starzewski, 1995; Dhaliwal and Singh, 1987). Complex media can be rightfully divided into three main groups: strain gradient elastic (Mindlin, 1964; 1965; Chen and Wang, 2001; Lam et al., 2003), surface elastic (Gurtin and Murdoch, 1975, 1978; Zhu et al., 2017; Huang, 2018) and finally micropolar elastic media (Toupin, 1962, 1964; Mindlin and Tiersten, 1962; Mindlin, 1963, 1964; Eringen, 1966). For the treatment of contact mechanics problems at the small scale, the Gurtin-Murdoch surface elasticity (GMSE) (Gurtin and Murdoch, 1975, 1978) and the couple stress elasticity (CSE) theories have been successfully employed with good results in terms of correlation with the experimental findings. One of the simplest classes of micropolar theory is the indeterminate couple stress theory (Koiter, 1964), which is essentially a gradient type (i.e. weakly) non-local theory where the deformation field at a point is related to its close neighborhood. This special theory assumes that the microrotations at each material point are coincident with the macroscopic rotations, i.e. the mean rotation of the principal axes of strain. In addition to the familiar stress and strain fields of classical elasticity, the couple stress theory employs the curvature and couple stress tensors as conjugated field variables. These are connected in constitutive terms through a characteristic length scale, which introduces the sought-for scale effect (Liu and Su, 2009). Typical values of the characteristic length can be found in Lakes (1986, 1993) for foam materials, in Chang et al. (2003) for granular materials, in Casolo (2006) for masonry, in Yang and Lakes (1982) for bone, in Nikolov et al. (2007) for glassy and semi-crystalline polymers.

Lately, the indeterminate couple stress theory of elasticity was successfully applied to fracture mechanics (Radi, 2007; Radi, 2008; Morini et al., 2013; Gourgiotis and Georgiadis, 2011; Nobili et al., 2019) and contact mechanics (Zisis et al., 2015; Gourgiotis and Zisis, 2016; Gourgiotis et al., 2016; Karuriya and Bhandakkar, 2017). Moreover, the effects of friction and adhesion on contact problems, within the framework of couple-stress elasticity, have been included in the works of Song et al. (2017), Wang et al. (2018) and Li and Liu (2020). There are several assumptions, especially concerning the new boundary conditions relating rotations and couple tractions, that were introduced in the solution of the above-mentioned problems in order to retrieve the classical elastic solution as the characteristic length of the microstruture tends to zero. For example, in contact problems involving a rigid punch, it is usually assumed that no (reduced) couple tractions are exchanged between the punch and the substrate when the latter is modelled as a classic Cauchy continuum. The aftermath of this questionable assumption is discussed in terms of Love wave propagation and it is shown that it leads to ill-posed problems (Nobili and Volpini, 2021).

Surprisingly, this assumption is generally introduced also when the substrate is a micropolar continuum (Zisis et al., 2014, 2018; Song et al., 2017) and therefore it is capable of supporting couple tractions. Similarly, Euler-Bernoulli (EB) beams in contact with a micropolar material are capable of exchanging distributed couples. These additional interactions are mechanically equivalent to an increment in the total contact pressure, in much the same way as the Kirchhoff equivalent shear stress encompasses the twisting moments in classical plate theory.

The plane problem of the bonded frictionless contact between a finite EB beam and a couple stress elastic half-plane has been recently investigated by Radi (2021) assuming that both normal stresses and couple tractions are transmitted along the contact zone. The interface conditions considered in that work assumes that both the slope and the rotation of the contacting bodies correspond.

In the present work, this novel contact scenario is extended to the much more involved situation of tensionless contact, thus allowing the beam to lift free from the half-plane and so parting the interaction zone in two disjoint sets defining contact and lift-off. Indeed, the special feature of unbonded contact, sometimes referred to as receding contact (Keer et al., 1972; El-Borgi et al., 2014; Yildirim et al., 2019), one-way contact (Attar et al., 2016), unilateral contact (Dempsey et al., 1984) or tensionless contact (Zhang and Liu, 2019), lies in allowing separation between the beam and the foundation. Following the debonding condition considered for a beam free to lift off from an elastic half-plane (Gladwell, 1976; Gallagher, 1983) and for a rigid indenter tilted over a couple stress elastic half-plane (Gourgiotis et al., 2016), it is here assumed that this separation kicks in when the contact pressure crosses the zero point. In general, the extension of the contact region is a problem unknown, that requires solving a nonlinear equation whose determination is not trivial (Nobili, 2012; Yilmaz et al., 2018). We show that this contact scenario implies that couple tractions are proportional to the derivative of the contact pressure along the contact zone, and thus, if the contact pressure is assumed to vanish as a square root at the contact ends, then couple tractions may exhibit a square root singularity therein.

The paper is organized as follows. The governing equations for the EB beam under a point load and the Green's functions for the couple-stress half-plane loaded by a concentrated force or couple are reported in Sections 2 and 3, respectively. The compatibility conditions between the beam and the half-plane surface are then presented in Section 4. They result in a pair of integral equations for the unknown distributions of contact pressure and couple tractions. One of these is of the Fredholm type and provides an analytical relation between the two unknown distributions. With this result, the second equation may be reduced in a form similar to that governing the classical contact problem between a beam and an elastic half-plane (Gladwell, 1976; Gallagher, 1983). An approximated procedure for reducing the last integral equation to an algebraic eigenvalue problem is then reported in Section 5, based on the expansion of the contact pressure in series of orthogonal Chebyshev polynomials of the second kind and then applying the collocation method. This procedure leads to a cubic eigenvalue problem which is approached by the linearization method. The variations of contact length with the material characteristic length of the foundation, as well

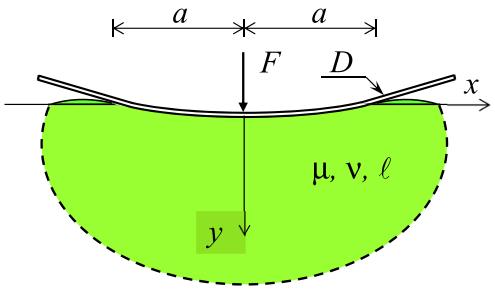

Fig. 1. A Euler-Bernoulli beam of flexural rigidity D in unbonded contact onto a couple stress elastic half-plane. The beam is acted upon by a concentrated load F at $x = 0$. The beam lifts-off from the foundation at $x = a$, being the beam length longer than $2a$.

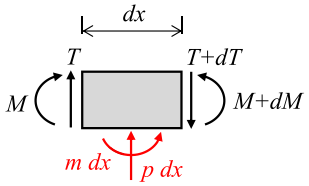

Fig. 2. Free body diagram of forces and couples acting on any infinitesimal beam element.

as the distributions of contact pressure, couple stress tractions, bending moment and shearing force along the beam are then illustrated in Section 6. Finally, the main conclusions are illustrated in Section 7.

2. Beam governing equations

Let us consider the plane strain problem of a uniform weightless elastic EB beam resting in unilateral frictionless contact onto a homogeneous isotropic elastic foundation. The beam has flexural rigidity D and is longer than the contact region. It is loaded, at midspan, by a transversal line load F applied at the origin of a Cartesian reference system $(0, x, y)$. This reference system is placed in such a manner that the x-axis corresponds to the undeformed beam axis while the y-axis is directed towards the foundation, as shown in Fig. 1.

As well known, translational and rotational equilibrium of any beam element (see Fig. 2) lends the balance equations for the shearing force T and the bending moment M in the beam, namely

$$T^{'}(x)–p(x)=0, \qquad M^{'}(x)-T(x)+m(x)=0, \tag{2.1}$$

where p and m are the contact pressure and the (reduced) couple stress tractions exchanged with the foundation. Hereinafter, prime denotes differentiation with respect to x.

According to the EB beam theory, the bending moment and the shearing force are connected by the constitutive assumptions to the derivatives of the beam deflection $v(x)$

$$M(x)=-D\,v^{''}(x), \qquad T(x)=-D\,v^{'''}(x)+m(x). \tag{2.2}$$

Together, Eq. (2.2) provide a single fourth-order linear differential equation

$$D\,v^{''''}(x)=m^{'}(x)-p(x). \tag{2.3}$$

Eqn (2.3) clearly shows that the effects of the couple tractions are equivalent to an additional contact pressure $-m'(x)$, as it occurs for the shearing force in the Kirchhoff plate theory. By exploiting the symmetry of the problem, we can focus on the right half of the beam corresponding to positive values of the abscissa x. Let us denote the abscissa of the edge of the contact zone with a (see Fig. 1, this is the point where the beam lifts off from the substrate), then the boundary conditions for the considered problem require that the bending moment and shearing force vanish at $x=a$, namely

$$M(a)=0, \qquad T(a)=0, \tag{2.4}$$

as well as

$$v^{'}(0)=0, \qquad T(0)=-F/2, \tag{2.5}$$

at $x=0$, due to the symmetry of the problem. Integrating eqn (2.3) between an arbitrary value of x, for $0\le x\le a$, and a, using eqn $(2.2)_2$ and the boundary conditions $(2.4)_2$, one obtains

$$Dv^{'''}(x)=\int_x^a p(t)dt+m(x). \tag{2.6}$$

Integrating eqn (2.6) between x and a again, and using eqn $(2.2)_1$ and the boundary conditions $(2.4)_1$, one has

$$Dv^{''}(x)=\int_x^a[(x-t)p(t)-m(t)\,]dt. \tag{2.7}$$

By integrating eqn (2.7) between 0 and x, using the boundary conditions $(2.5)_1$, after integration by parts it follows

$$Dv^{'}(x)=-\int_0^x\left[\frac{(x-t)^2}{2}p(t)-(x-t)m(t)\right]dt-x\int_0^a\left[\left(t-\frac{x}{2}\right)p(t)+m(t)\right]dt. \tag{2.8}$$

Moreover, the balance condition for the half beam yields

$$\int_0^a p(t)dt=\frac{F}{2}. \tag{2.9}$$

3. Substrate governing equations

The foundation is modelled as a homogeneous isotropic couple stress elastic half-plane under plane strain condition. Consequently, the classical strain field

$$\varepsilon_{xx}=u_{x,x}, \qquad \varepsilon_{yy}=u_{y,y}, \qquad \varepsilon_{xy}=\left(u_{x,y}+u_{y,x}\right)/2, \tag{3.1}$$

is supplemented by the curvature field

$$\kappa_{xz}=\omega_{z,x}, \qquad \kappa_{yz}=\omega_{z,y}, \tag{3.2}$$

where $\omega_z=(u_{y,x}-u_{x,y})/2$ is the microrotation vector. Here, $u_x(x, y)$ and $u_y(x, y)$ denote the in-plane displacement components and a subscript comma signifies partial differentiation with respect to the relevant variable, e.g. $u_{x,x}=\partial u_x/\partial x$. Note that clockwise rotation is considered positive. The balance equations read

$$\begin{aligned}\sigma_{xx,x}+\sigma_{yx,y}&=0,\\ \sigma_{xy,x}+\sigma_{yy,y}&=0,\\ \sigma_{xy}-\sigma_{yx}+m_{xz,x}+m_{yz,y}&=0,\end{aligned} \tag{3.3}$$

where $\boldsymbol{\sigma}$ and $\boldsymbol{m}$ are the Cauchy and the couple stress tensor, respectively. As for classical isotropic elastic materials, the constitutive relations between stresses and strains for isotropic couple stress elastic materials under plane strain conditions are defined by two scalar parameters, namely the shear modulus μ and the Poisson ratio ν,

$$\begin{aligned}\varepsilon_{xx}&=\left[(1-\nu)\,\sigma_{xx}-\nu\,\sigma_{yy}\right]/(2\mu),\\ \varepsilon_{yy}&=\left[(1-\nu)\,\sigma_{yy}-\nu\,\sigma_{xx}\right]/(2\mu),\\ \varepsilon_{xy}&=\left(\sigma_{xy}+\sigma_{yx}\right)/(4\mu).\end{aligned} \tag{3.4}$$

The additional constitutive relation between couple stresses and curvatures requires an additional material parameter, namely the material characteristic length ℓ

$$\kappa_{xz}=\frac{m_{xz}}{4\mu\ell^2}, \qquad \kappa_{yz}=\frac{m_{yz}}{4\mu\ell^2}. \tag{3.5}$$

3.1. Green's functions for the foundation

The normal displacement, slope and microrotation at the surface of a couple stress homogenenous isotropic elastic half-plane were derived by Radi (2021) for a clockwise couple C acting at the origin of the coordinate system

$$u_y^C(x,0)=C\frac{1-\nu}{\pi\mu}\int_0^\infty w(s\ell)\sin sx\,ds, \tag{3.6}$$

$$u^{C}_{y,x}(x,0) = C\frac{1-\nu}{\pi\mu}\int_0^\infty w(s\ell)s\cos sx\, ds, \tag{3.7}$$

$$\omega^{C}_{z}(x,0) = C\frac{1-\nu}{\pi\mu\ell}\int_0^\infty w(s\ell)\left[s\ell + \frac{s\ell+\sqrt{1+s^2\ell^2}}{4\,(1-\nu)}\right]\cos sx\, ds, \tag{3.8}$$

respectively, where the following shorthand are introduced

$$w(z) = \frac{\sqrt{1+z^2}-z}{g(z)}, \tag{3.9}$$

and

$$g(z) = \sqrt{1+z^2} + 4(1-\nu)z^2\left(\sqrt{1+z^2}-z\right). \tag{3.10}$$

Note that the function $g(z)$ behaves as $(3-2\nu)\,z + O(z)$ as $z \to \infty$ and consequently, the function $w(z)$ behaves as $O(z^{-2})$ as $z \to \infty$, by which fact the rotation ω^{C}_{z} displays a logarithmic singularity under the loading couple.

Similarly, the normal displacement, slope and rotation fields due to the application of a normal point force P at the origin of the coordinate reference system can be found in Gourgiotis and Zisis (2016), Zisis et al. (2018), and Radi (2021), namely

$$u^{P}_{y}(x,0) = \frac{P}{\pi\mu}(1-\nu)\int_0^\infty \frac{\sqrt{1+s^2\ell^2}}{s\,g(s\ell)}\cos sx\, ds, \tag{3.11}$$

$$\begin{aligned} u^{P}_{y,x}(x,0) &= -\frac{P}{\pi\mu}(1-\nu)\int_0^\infty \frac{\sqrt{1+s^2\ell^2}}{g(s\ell)}\sin sx\, ds = \\ &= \frac{P}{\pi\mu}\frac{1-\nu}{3-2\nu}\left[-\frac{1}{x} + 2(1-\nu)\int_0^\infty f(s\ell)\sin sx\, ds\right], \end{aligned} \tag{3.12}$$

$$\omega^{P}_{z}(x,0) = -P\frac{1-\nu}{\pi\mu}\int_0^\infty w(s\ell)\sin sx\, ds, \tag{3.13}$$

where

$$f(z) = \left[2z^2\left(\sqrt{1+z^2}-z\right) - \sqrt{1+z^2}\right]\Big/ g(z), \tag{3.14}$$

so that $f(z)$ behaves as $O(z^{-2})$ as $z \to \infty$, and $f(0) = -1$.

4. Contact conditions

We are now in a position to write the contact conditions connecting the beam to the supporting foundation. These conditions require that no shear stress nor tensile tractions develop at the interface, while the same deflection stands for the beam and for the foundation surface along the contact region.

The condition concerning frictionless contact is warranted by the Green's functions introduced in Section 3. Besides, deflection compatibility can be advantageously formulated in terms of slope, which step disposes of any additional rigid body displacement. This complementarity problem spells out as

$$v'(x) = u_{y,x}(x,0), \qquad \text{for } |x| \le a, \tag{4.1}$$

$$u_{y,x}(x,0) = \omega_z(x,0), \qquad \text{for } |x| \le a \tag{4.2}$$

and, clearly, $p(x) = m(x) = 0$ for $|x| > a$.

The contact conditions (4.2) stipulating coincidence between micro and macro-rotations, entails that $u_{x,y} + u_{y,x} = 0$, namely there is no surface shear deformation $\varepsilon_{xy} = 0$. Then, according to the frictionless assumptions both shear stress components σ_{xy} and σ_{yx} in the foundation are also vanishing along the contact zone.

Using the Green functions, we can easily write the kinematical conditions (4.1) and (4.2) in terms of the distribution of contact pressure $p(x)$ and couple tractions $m(x)$ being exchanged between the beam and the foundation. To this aim, we need the following expressions for the slope $u_{y,x}(x, 0)$ and the rotation $\omega_z(x, 0)$ of the foundation surface, that are obtained from the Green's functions (3.7), (3.8), (3.12) and (3.13)

$$\begin{aligned} u_{y,x}(x,0) = \frac{1-\nu}{\pi\mu}\Bigg\{ &-\int_{-a}^{a} p(t)dt\int_0^\infty \frac{\sqrt{1+s^2\ell^2}}{g(s\ell)}\sin[s(x-t)]ds \\ &+\int_{-a}^{a} m(t)dt\int_0^\infty w(s\ell)s\cos[s(x-t)]ds\Bigg\}, \end{aligned} \tag{4.3}$$

$$\begin{aligned} \omega_z(x,0) = \frac{1-\nu}{\pi\mu}\Bigg\{ &-\int_{-a}^{a} p(t)dt\int_0^\infty w(s\ell)\sin[s(x-t)]ds \\ &+\int_{-a}^{a} m(t)dt\int_0^\infty w(s\ell)\left[s + \frac{s\ell+\sqrt{1+s^2\ell^2}}{4\,(1-\nu)\,\ell}\right]\cos[s(x-t)]ds\Bigg\} \end{aligned} \tag{4.4}$$

Therefore, introduction of eqns (4.3) and (4).4) into the contact condition (4.2) provides the following integral equation

$$\int_{-a}^{a} p(t)dt\int_0^\infty \frac{s\,\sin[s(x-t)]}{g(s\ell)}ds + \int_{-a}^{a} m(t)dt\int_0^\infty \frac{\cos[s(x-t)]}{4(1-\nu)\ell^2 g(s\ell)}ds = 0, \tag{4.5}$$

for $|x| \le a$. Note that, integrating by parts and using the lift-off conditions $p(\pm a) = 0$, one has

$$s\int_{-a}^{a} p(t)\sin[s(x-t)]dt = -\int_{-a}^{a} p'(t)\cos[s(x-t)]dt. \tag{4.6}$$

Then, by using the result (4.6) in eqn (4.5), it follows that

$$\int_{-a}^{a}\left[p'(t) - \frac{m(t)}{4(1-\nu)\ell^2}\right]dt\int_0^\infty \frac{\cos[s(x-t)]}{g(s\ell)}ds = 0, \tag{4.7}$$

for $|x| \le a$. where Note that the term within square brackets is odd with respect to t. Then, according to the result in Appendix D, equation (4.7) necessarily implies that

$$m(t) = 4(1-\nu)\ell^2 p'(t). \tag{4.8}$$

The introduction of eqns (2.8) and (4).3) into the contact condition (4.1), by using the results (4.8) and (4.6), recalling also the definitions (3.9) and (3.10) of the functions w and d and the definite integral

$$\int_0^\infty \sin[s(x-t)]ds = \frac{1}{x-t}, \tag{4.9}$$

then gives the following integral equation

$$\int_0^x\left[\frac{(x-t)^2}{2} - 4(1-\nu)\ell^2\right]p(t)dt + x\int_0^a\left(t-\frac{x}{2}\right)p(t)dt = D\frac{1-\nu}{\mu\pi}\int_{-a}^{a}\frac{p(t)}{x-t}dt, \tag{4.10}$$

for $|x| \le a$. This homogeneous integral equation closely resembles that governing the problem of the tensionless contact between a beam and a *classical* elastic half-plane, as it appears in Gladwell (1976) and Gallagher (1983), with the remarkable exception of the term containing the characteristic length ℓ of the material. It is therefore trivial to deduce the classical case letting $\ell \to 0$. It is important to observe that this integral equation hides the contact length a inside the integral limits. Introducing the dimensionless variables $\xi = x/a$ and $\tau = t/a$ we bring it out

$$\int_0^{\xi}\left[\frac{(\xi-\tau)^2}{2}-4\,(1-\nu)\frac{\ell^2}{a^2}\right]p(\tau)d\tau+\xi\int_0^{1}\left(\tau-\frac{\xi}{2}\right)p(\tau)d\tau=\frac{L^3}{\pi a^3}\int_{-1}^{1}\frac{p(\tau)}{\xi-\tau}d\tau, \tag{4.11}$$

for $|\xi|\leq 1$, in what is a cubic eigenvalue problem for the contact length a, where the length L is defined by

$$L=\sqrt[3]{\frac{1-\nu}{\mu}}D. \tag{4.12}$$

As expected, this dependence of the eigenvalue reveals that for $a\gg\ell$ the classical problem dominates, while for $a\sim\ell\ll 1$, the term of couple stress origin in (4.11) provides a significant contribution.

4.1. Numerical solution by the collocation method

At the ends of the contact region, namely at $x=\pm a$, the pressure $p(a)$ must vanish as required by the lift-off condition. Accordingly, we write the contact pressure in the form of a Chebyshev series using the Chebyshev polynomials of the second kind U_{2n}. Here, owing to the symmetric setup, we only use even terms (see Appendix A),

$$p(x)=\frac{F}{a}\sum_{n=0}^{\infty}p_n U_{2n}\left(\frac{x}{a}\right)\sqrt{1-\left(\frac{x}{a}\right)^2}, \tag{4.13}$$

for $|x|\leq a$, where p_n ($n=0, 1, 2, \ldots$) are coefficients to be determined by collocation. Then, according to the result (4.8), the couple tractions $m(a)$ displays singular behavior at the edge of the contact zone, namely

$$m(x)=-4(1-\nu)\frac{F\ell^2}{a^2}\sum_{n=0}^{\infty}(1+2n)p_n\frac{T_{2n+1}(x/a)}{\sqrt{1-(x/a)^2}}, \tag{4.14}$$

for $|x|\leq a$, where T_{2n+1} are the Chebyshev polynomials of the first kind, this time of odd order $2n+1$ (see Appendix A). In other words, the contract pressure is an even function of x, while the couple tractions are odd. By using the result (A.2) provided in Appendix A, being $U_0(t)=1$, the introduction of representations $(4.13)_1$ in the balance condition (2.9) provides the first coefficient

$$p_0=2/\pi. \tag{4.15}$$

The introduction of representations (4.13) in eqn (4.11) together with the non-dimensional parameters

$$\lambda=\ell/L,\qquad \beta=a/L, \tag{4.16}$$

using the result (A.3), then yields a homogeneous equation for the unknown coefficients p_n ($n=0, 1, \ldots, N$)

$$\sum_{n=0}^{\infty}\left[T_{2n+1}(\xi)+4(1-\nu)\lambda^2\beta C_{2n}^{(0)}(\xi)-\beta^3 A_n(\xi)\right]p_n=0, \tag{4.17}$$

for $0\leq\xi\leq 1$, where the function $A_n(\xi)$ is given by

$$A_n(\xi)=\frac{1}{2}\left[\xi^2 C_{2n}^{(0)}(\xi)-2\xi C_{2n}^{(1)}(\xi)+C_{2n}^{(2)}(\xi)+2\xi C_{2n}^{(1)}(1)-\xi^2 C_{2n}^{(0)}(1)\right], \tag{4.18}$$

for $n\geq 0$, being

$$C_n^{(m)}(\xi)=\int_0^{\xi}U_n(\tau)\sqrt{1-\tau^2}\,\tau^m\,d\tau. \tag{4.19}$$

Closed form expressions for the definite integral (4.19) are worked out in Appendix B for $m=0, 1, 2$. Note that, the size a of the contact region and thus the parameter β defined in (4.16) are unknowns. Moreover, the parameter β is an eigenvalue of the cubic eigenvalue problem (4.17) satisfying the balance condition (4.15), which provides a normalization condition for the eigenvalue problem.

5. Approximate solution

In order to transform the compatibility condition (4.17) into a linear homogeneous system of $N+1$ algebraic equations for the unknown coefficients p_n (for $n=0, 1, 2, \ldots, N$), a collocation procedure is introduced by truncating series (4.13) to the first $N+1$ terms. Their coefficients are determined imposing the compatibility condition (4.17) at $N+1$ collocation points ξ_k ($k=0, 1, 2, \ldots, N$), ranging between 0 and 1, selected as the positive roots of the Chebyshev polynomial $T_{2N+2}(\xi)$, namely

$$\xi_k=\cos\frac{(2k+1)\pi}{4(N+1)},\qquad \text{for } k=0, 1, \ldots, N. \tag{5.1}$$

To this aim, let us define the following components of the $(N+1)\times(N+1)$ matrices $\mathbf{T}$, $\mathbf{B}$ and $\mathbf{A}$

$$T_{kn}=T_{2n+1}(\xi_k),\qquad B_{kn}=4(1-\nu)\lambda^2 C_{2n}^{(0)}(\xi_k),\qquad A_{kn}=A_n(\xi_k), \tag{5.2}$$

for $n, k=0, 1, 2, \ldots, N$. Then, the homogeneous equation (4.17) provides the following algebraic system

$$\left(\mathbf{T}+\beta\,\mathbf{B}-\beta^3\,\mathbf{A}\right)\mathbf{p}=\mathbf{0}, \tag{5.3}$$

where the upper-case bold symbols denote $(N+1)\times(N+1)$ square matrices and the lower-case bold symbols denote vectors of $N+1$ components. The homogeneous algebraic equation (5.3) together with the balance condition (4.15) defines a generalized cubic eigenvalue problem for the eigenvalue β and eigenvector $\mathbf{p}$, which can be reduced to the following enlarged linear eigenvalue problem

$$\begin{bmatrix}\mathbf{0}&\mathbf{I}&\mathbf{0}\\ \mathbf{0}&\mathbf{0}&\mathbf{I}\\ \mathbf{T}&\mathbf{B}&\mathbf{0}\end{bmatrix}\begin{pmatrix}\mathbf{p}\\ \beta\,\mathbf{p}\\ \beta^2\,\mathbf{p}\end{pmatrix}=\beta\begin{bmatrix}\mathbf{I}&\mathbf{0}&\mathbf{0}\\ \mathbf{0}&\mathbf{I}&\mathbf{0}\\ \mathbf{0}&\mathbf{0}&\mathbf{A}\end{bmatrix}\begin{pmatrix}\mathbf{p}\\ \beta\,\mathbf{p}\\ \beta^2\,\mathbf{p}\end{pmatrix}, \tag{5.4}$$

where $\mathbf{0}$ and $\mathbf{I}$ are the $(N+1)\times(N+1)$ null matrix and identity matrix, respectively. The procedure then takes the smallest real and positive eigenvalue β of the generalized eigenvalue problem (5.4) and the corresponding eigenvector $\mathbf{p}$ that provide a positive (compressive) distribution of pressure $(4.13)_1$ under the beam for $|x|<a$, where $a=\beta L$.

Once the eigenvector $\mathbf{p}$ is known, the contact pressure and couple tractions under the beam immediately follow from (4.13) and (4.14). The bending moment and shearing force along the beam, for $0\leq x\leq a$, can be obtained from eqns (2.2) and (2.8) by using (4.8), as

$$M(x)=-\int_x^a[(x-t)p(t)-m(t)]dt=-\int_x^a(x-t)p(t)dt-4(1-\nu)\ell^2 p(x), \tag{5.5}$$

$$T(x)=-\int_x^a p(t)\,dt. \tag{5.6}$$

Then, introducing the series expansions (4.13) and (4.14) and the normalized variables $\xi=x/a$ and $\tau=t/a$, it follows that

$$\frac{M(\xi)}{Fa}=-\sum_{n=0}^{\infty}p_n\left[\int_{\xi}^{1}U_{2n}(t)\sqrt{1-\tau^2}\,(\xi-\tau)d\tau+4(1-\nu)\frac{\lambda^2}{\beta^2}U_{2n}(\xi)\sqrt{1-\xi^2}\right], \tag{5.7}$$

$$\frac{T(\xi)}{F}=-\sum_{n=0}^{\infty}p_n\int_{\xi}^{1}U_{2n}(\tau)\sqrt{1-\tau^2}\,d\tau. \tag{5.8}$$

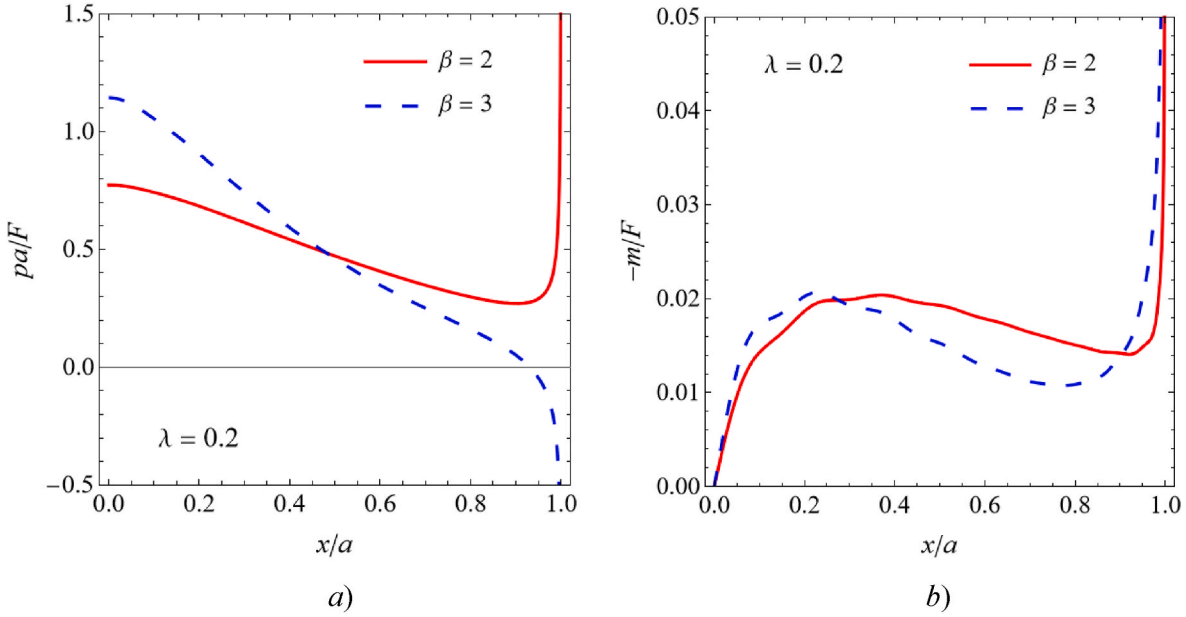

Fig. 3. Contact pressure (*a*) and couple tractions (*b*) exchanged between a beam and a couple stress half-plane in bilateral frictionless contact. Here, $\nu = 0.3$, $\lambda = \ell/L = 0.2$, and two values of the normalized beam length $\beta = a/L$ are considered, (*a*) smaller and (*b*) greater than the critical length ($\beta = 2.42$). In the former case the contact pressure is positive throughout, and thus compressive, in the latter it attains negative values which indicate tensile stress tractions.

Plugging the series representations (4.13), truncated to N terms, into eqns (5.7) and (5).8), then yields

$$\frac{M(\xi)}{Fa} = \sum_{n=0}^{N} p_n \left[\xi C_{2n}^{(0)}(\xi) - \xi C_{2n}^{(0)}(1) - C_{2n}^{(1)}(\xi) + C_{2n}^{(1)}(1) + 4(1 - \nu)\frac{\lambda^2}{\beta^2} U_{2n}(\xi)\sqrt{1-\xi^2} \right], \tag{5.9}$$

$$\frac{T(\xi)}{F} = -\sum_{n=0}^{N} p_n \left[C_{2n}^{(0)}(1) - C_{2n}^{(0)}(\xi) \right], \tag{5.10}$$

for $0 \le \xi \le 1$. The functions $C_n^{(m)}$ are defined in eqn (4.19) and explicitly calculated in Appendix B.

5.1. *Special case for vanishing couple tractions*

If the couple tractions are vanishing under the beam, then the problem reduces to the single equation (4.1), which requires continuity of slope between the beam and the foundation. In this case, the rotation of the half-plane surface $\omega_z(x, 0)$ is free. Then, by introducing eqns (4.3) and (2).8) for $m = 0$ in condition (4.1), one has

$$\int_0^x \frac{(x-t)^2}{2} p(t)dt + x\int_0^a \left(t - \frac{x}{2}\right) p(t)dt = D\frac{1-\nu}{\mu\pi} \int_{-a}^{a} p(t)dt \int_0^{\infty} \frac{\sqrt{1+s^2\ell^2}}{g(s\ell)} \sin[s(x-t)]ds, \tag{5.11}$$

for $|x| \le a$. The introduction of the Chebyshev series (4.13) for the contact pressure in eqn (5.11), using the integral (A.4), then yields

$$\sum_{n=0}^{\infty} [F_n(\xi) - \beta^3 A_n(\xi)] p_n = 0, \quad \text{for } 0 \le \xi \le 1, \tag{5.12}$$

where the function $A_n(\xi)$ has been defined in (4.18) and

$$F_n(\xi) = (2n+1)(-1)^n \int_0^{\infty} \frac{\sqrt{1+\alpha^2\Lambda^2}}{\alpha\, g(\alpha\Lambda)} J_{2n+1}(\alpha) \sin\alpha\xi \, d\alpha, \tag{5.13}$$

being $\Lambda = \ell/a$. The functions $F_n(\xi)$ for $n = 0, 1, 2, \ldots$defined in (5.13) involve infinite integrals of highly oscillatory functions given by the product of trigonometric and Bessel functions. They are calculated accurately by using a special numerical integration procedure based on contour integration in the complex plane, as illustrated in Appendix C.

By using a collocation procedure similar to that used in section 5, equation (5.12) is then transformed into a homogeneous system of linear algebraic equations for the unknown coefficients p_n, $n = 0, 1, 2, \ldots, N$, which has the form of a generalized linear eigenvalue problem for the eigenvalue β^3, namely

$$(\mathbf{F} - \beta^3 \mathbf{A})\mathbf{p} = \mathbf{0}. \tag{5.14}$$

Here, the $(N+1) \times (N+1)$ square matrix $\mathbf{F}$ has the components

$$F_{kn} = F_n(\xi_k), \qquad \text{for } n, k = 0, 1, \ldots, N. \tag{5.15}$$

Introducing the series expansion (4.13) into eqns (5.5) and (5).6), while letting $m = 0$, yields the bending moment and shearing force along the beam

$$\frac{M(\xi)}{Fa} = \sum_{n=0}^{N} p_n \left[\xi C_{2n}^{(0)}(\xi) - \xi C_{2n}^{(0)}(1) - C_{2n}^{(1)}(\xi) + C_{2n}^{(1)}(1) \right], \tag{5.16}$$

$$\frac{T(\xi)}{F} = -\sum_{n=0}^{N} p_n \left[C_{2n}^{(0)}(1) - C_{2n}^{(0)}(\xi) \right], \tag{5.17}$$

for $0 \le \xi \le 1$, where the functions $C_n^{(m)}$ are defined in eqn (4.19) and they

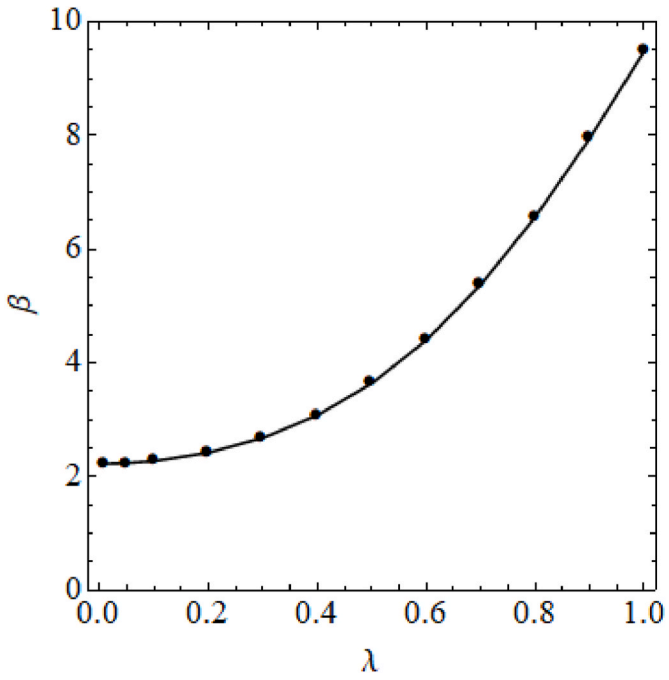

Fig. 4. Dimensionless contact length $\beta = a/L$ as a function of the normalized characteristic length $\lambda = \ell/L$ for the tensionless contact problem, ($\nu = 0.3$).

are calculated analytically in Appendix B.

6. Results and discussion

The first step in our analysis is to relate this problem to that of the beam in full contact with the substrate, which situation has been considered by Radi (2021) revealing that both stresses and couple tractions are square root singular at the beam ends. Hereinafter, we consider $\nu = 0.3$ for the Poisson's coefficient and $N = 20$ for the number of collocation points.

In Fig. 3 we plot the contact pressure and the couple traction distribution for a beam of length $2a$ in full contact with the substrate, for $\lambda = \ell/L = 0.2$ and $\nu = 0.3$. These curves show that the contact pressure due to a centred point load is fully compressive under the beam if the beam is shorter than some critical length, e.g. for $\beta = 2$, while tensile stress tractions start to appear if the beam is longer, e.g. for $\beta = 3$. Indeed, as found in the following, this critical length, which marks the appearance of lift-off, is located at $\beta = 2.42$ (assuming, as in Fig. 3, that $\lambda = 0.2$). Fig. 3*b* shows that the couple tractions are singular at the beam ends and have the same sign irrespectively of the beam being shorter or longer than the critical length, namely, both for $\beta = 0.2$ and $\beta = 0.3$. It follows that, in the tractionless contact framework, the contact pressure must vanish at the lift-off points, where the couple tractions are expected to exhibit a square root singularity, as assumed in (4.13) and (4.14).

The variation of the critical length β relating the contact length a to the beam length L, defined in (4.16), is plotted in Fig. 4 for tensionless contact as a function of the normalized characteristic length λ for the half-plane. This curve shows that the contact length increases with λ due to the effects of the couple tractions, which contribute to keeping the beam in contact with the half-plane, especially at the ends of the contact zone. As the material characteristic length becomes vanishingly small, it can be also observed that the contact length a tends to recover the prediction of Gladwell (1976) and Gallagher (1983) for the standard elastic contact problem, who obtained $a/L = 11.07^{1/3} = 2.229$ and $a/L = 11^{1/3} = 2.224$, respectively. Numerical results are also presented in Table 1.

The normalized distributions of contact pressure and couple traction under the beam are plotted in Fig. 5 for five values of the characteristic length of the elastic half-plane as it compares with the beam length. In

Table 1
Values of the normalized contact length $\beta = a/L$ for some values of the normalized characteristic length $\lambda = \ell/L$, for $\nu = 0.3$ in the presence of couple tractions.

λ	0.01	0.05	0.10	0.20	0.30	0.40	0.50	0.60	0.70	0.80	0.90	1.00
β	2.226	2.237	2.273	2.421	2.682	3.080	3.643	4.403	5.380	6.572	7.954	9.486

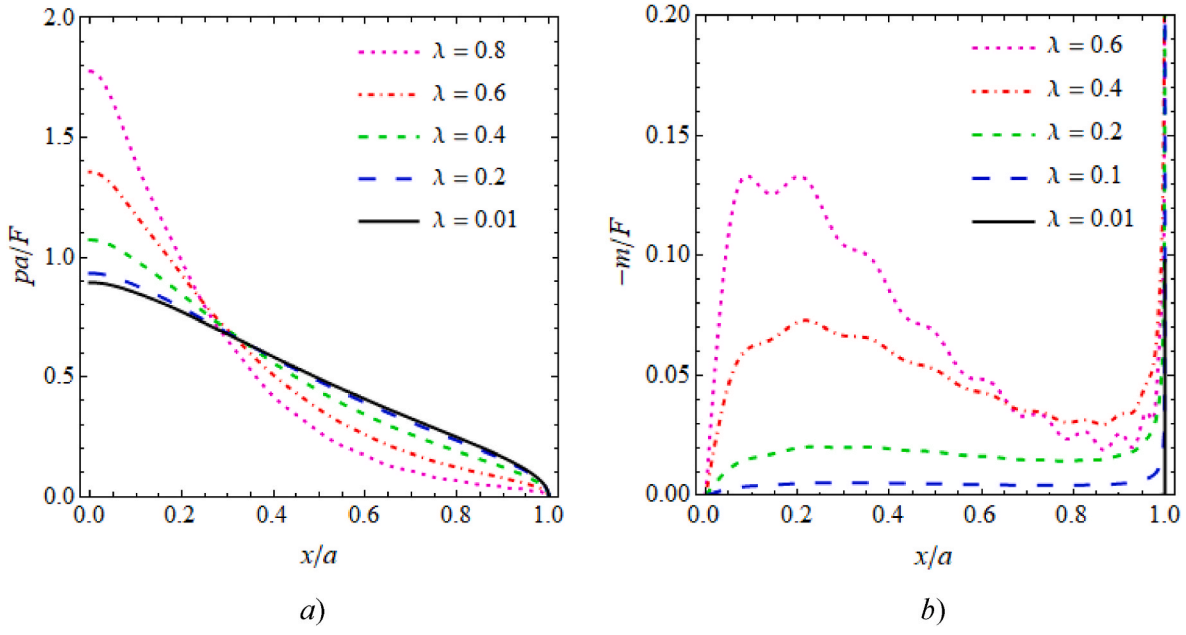

Fig. 5. Contact pressure (a) and couple tractions (b) as a function of dimensionless position in the contact region for the tensionless contact problem, at $\nu = 0.3$ and for five different values of the relative length scale in the foundation, $\lambda = \ell/L$.

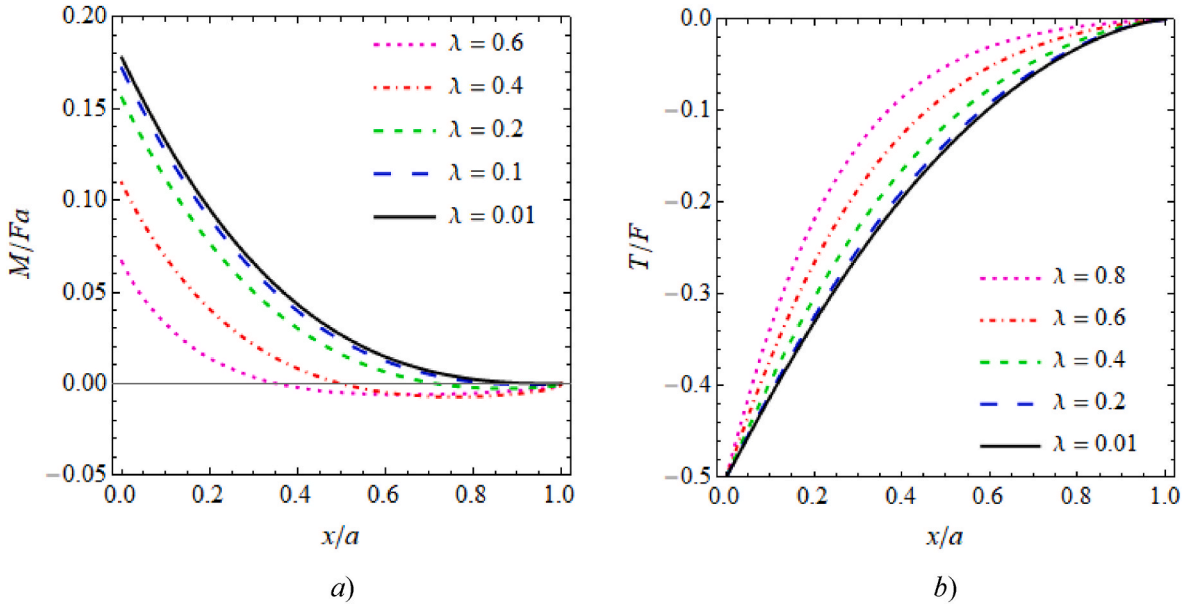

Fig. 6. Bending moment (*a*) and shearing force (*b*) along the contact zone, for five values of the characteristic parameter $\lambda = \ell/L$ ($\nu = 0.3$).

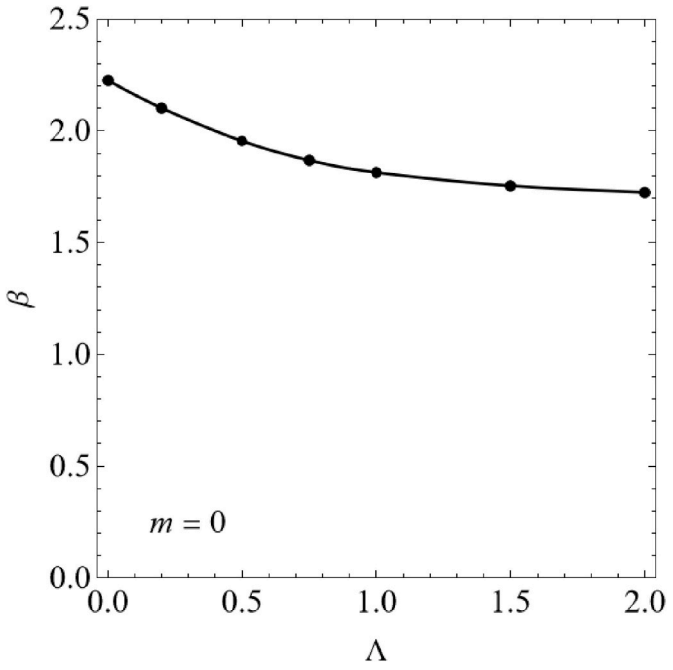

Fig. 7. Dimensionless contact length $\beta = a/L$, as a function of the relative length scale of the microstructure $\Lambda = \ell/a$ in the absence of couple tractions along the contact zone, for $\nu = 0.3$.

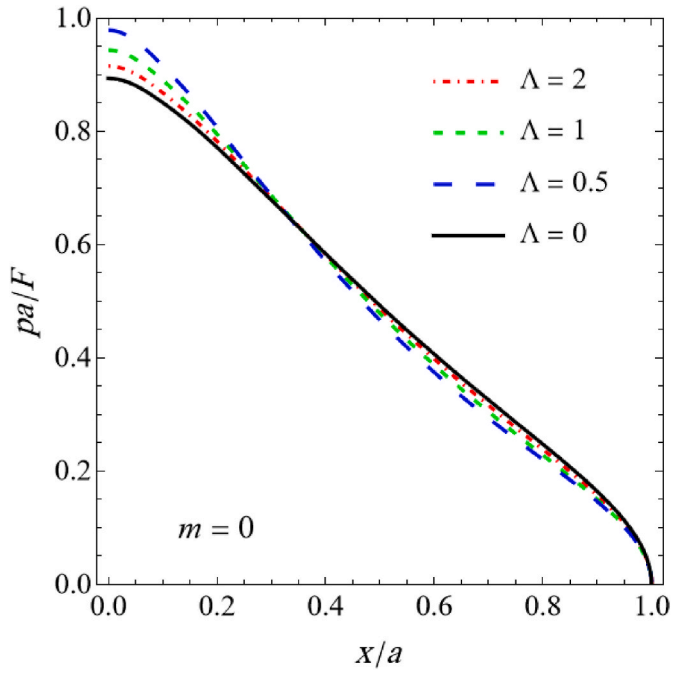

Fig. 8. Contact pressure distribution along the contact zone for four values of the relative lengthscale $\Lambda = \ell/a$, in the absence of couple tractions exchange ($\nu = 0.3$).

Fig. 5*a*, it can be observed that the contact pressure under the beam is compressive, attains its maximum at the point of application of the line load and correctly vanishes at the lift-off point. Moreover, for a very small characteristic length, e. g. for $\lambda = 0.01$, the curve approaches the classical elastic solution. As the normalized characteristic length λ increases, the magnitude of contact pressure increases strongly in the neighborhood of the loading and fades off rapidly approaching the end of the contact zone. In all curves, the couple tractions plotted in Fig. 5*b* display a singular behavior at the end of the contact zone and equally increase for higher values of the characteristic length λ. Notably, as the parameter λ increases, oscillations appear in the distribution of the couple tractions, which may be reduced increasing the number of terms (N+1) considered in the approximation (4.13). This behavior is an indicator of the unstable character of the couple tractions for large material characteristic lengths. Conversely, as the characteristic length becomes vanishingly small, the couple tractions under the beam tend to disappear and localize at the contact end: in this sense, the contact pressure approaches but never recovers the classical elastic solution.

The corresponding normalized distributions of bending moment and shearing force along the beam are plotted in Fig. 6. As expected, the bending moment peaks under the line load, where the shearing force jumps. The effect of increasing the microstructure lengthscale consists of a considerable reduction of the bending moment peak under the load and a mild increment in the shearing force (in absolute terms). This

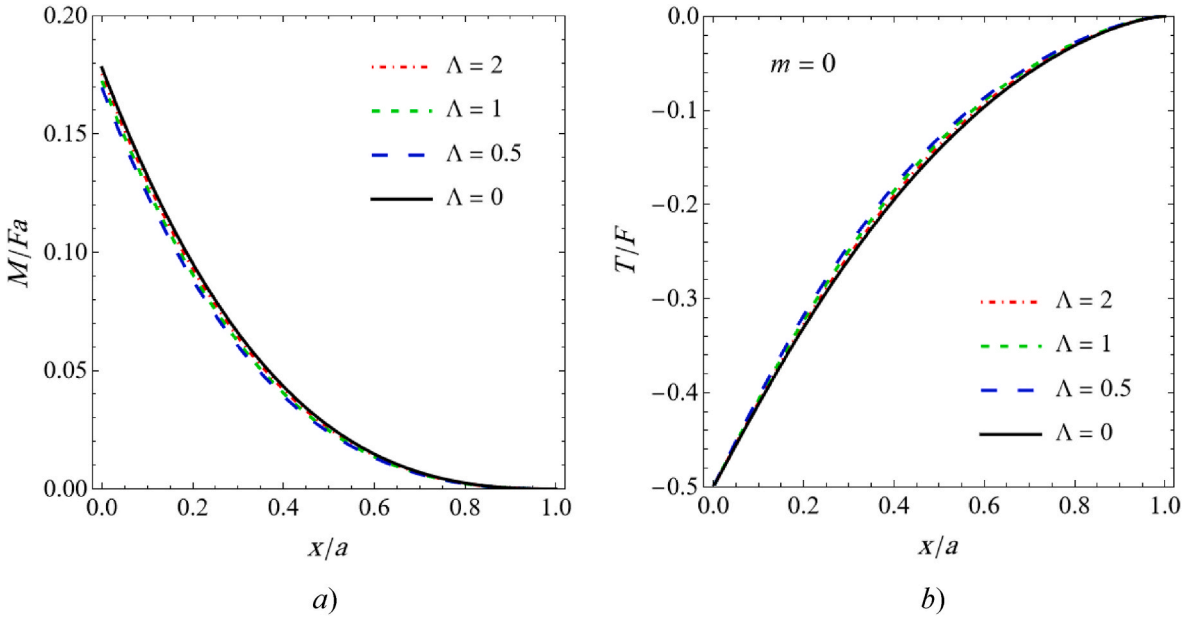

Fig. 9. Bending moment (a) and of the shearing force (b) distribution along the contact zone, for four values of the relative lengthscale $\Lambda = \ell/a$, in the absence of couple tractions exchange ($\nu = 0.3$).

Table 2
Values of the normalized contact length $\beta = a/L$ for some values of the normalized characteristic length $\lambda = \ell/L$, for $\nu = 0.3$ in the absence of couple tractions.

λ	0	0.2	0.5	1.0	1.5	2.0
B	2.225	2.102	1.954	1.814	1.754	1.725

suggests that consideration of the microstructure and of the couple stress exchange with the foundation considerably relieves the beam from the bending stress. In particular, due to the contribution of the couple tractions, the bending moment occurs with opposite sign at the lift-off points, thereby promoting adhesion to the foundation.

For the sake of comparison, the results obtained under the alternative assumption of vanishing couple tractions under the beam, already introduced in Section 5.1, are plotted in Figs. 7–9. In particular, the variation of the critical ratio β between the contact length a and the length L with the normalized characteristic length of the half-plane $\Lambda = \ell/a$ is plotted in Fig. 7. Similar results are also reported in Table 2. Interestingly, the dimensionless contact length β appears to decrease as the normalized characteristic lengthscale Λ increases, in contrast with the behaviour observed in Fig. 4 obtained in the presence of couple tractions along the contact zone. Note that the lengthscale Λ adopted here is normalized against the contact length a, as opposed to the parameter λ previously introduced which is normalized with respect to the beam half-length L.

The contact pressure distribution under the beam is shown in Fig. 8 for four values of the non-dimensional ratio Λ, in the absence of couple traction exchange. In this simplified contact scenario, the characteristic length of the material affects the contact pressure very little, in sharp contrast with the results observed in Fig. 5a for the case when couple tractions are acting. Also, no uniform trend can be retrieved. Equally, the bearing of the material characteristic length on the distribution of bending moment and shearing force along the beam, which is illustrated in Fig. 9a and 9b, respectively, is very mild, compared to that described in Fig. 6. Therefore, it may be concluded that the presence of the couple tractions under the beam is the main driver of the size effect observed in the contact problem between a beam and an elastic half-plane with microstructure. Consequently, ignoring couple tractions amounts to greatly underestimating the effect of the microstructure and results closely match the classical contact scenario.

7. Conclusions

In this paper, the contact problem for a beam resting in unilateral contact onto a microstructured foundation is investigated. The problem is formulated in terms of a single cubic eigenvalue problem for linear integral operators of the difference type. The contact evolution that emerges is the natural continuation of progressing from a beam in complete contact with the substrate until separation kicks in, with the contact pressure vanishing at the lift-off points and the couple tractions developing a square root singularity. Significantly, couple stresses appear as the main contributor to the deviation of the results from the classical scenario, that neglects the internal characteristic lengthscale. In this respect, neglecting couple stress exchange between the beam and the substrate greatly mitigates the role played by the microstructure in affecting the contact mechanics. In particular, accounting for the microstructure yields a contact pressure distribution that is highly peaked about the load application point. This outcome is much stronger than that obtained from classical elasticity and also compared to the case, often met in the literature, when couple tractions are not transmitted along the contact zone.

In fact, besides the usual compatibility between the slope of the two solids in contact, here we also require compatibility between the rotations of the foundation surface and of the beam mid-plane. This has profound consequences on the contact pattern, in terms of exchanged forces and resulting stresses, as well as on the contact length. Indeed, a striking feature predicted by the present solution is the remarkable size-effect affecting the magnitude of the contact pressure and, in turn, the bending moment, when the intrinsic characteristic length scale of the ground becomes comparable to the length of the contact zone. Results may be very significant when designing micro- and nano-scale devices, for then the contact pressure predicted by the classical theory is much underestimated. Finally, it must be remarked that the plane strain condition here considered is strictly valid for a long strip or plate extending in the out of plane direction, and thus the results here presented are approximated for a beam of small width. A fully three-dimensional analysis of this contact problem will be the subject of further investigations.

Declaration of competing interest

The authors declare the following financial interests/personal relationships which may be considered as potential competing interests: Radi Enrico reports financial support was provided by Government of Italy Ministry of Education University and Research. Nobili Andrea reports financial support was provided by Government of Italy Ministry of Education University and Research.

Data availability

Data will be made available on request.

Acknowledgements

Financial support within the framework of the grant MIUR-PRIN2020 "Mathematics for industry 4.0" (code 2020F3NCPX) is gratefully acknowledged. This research has been performed within the framework of the grant MIUR-PRIN 2020F3NCPX "Mathematics for industry 4.0 (Math4I4)'' ER and AN gratefully acknowledge support from MSCA-RISE-2020 project EffectFact https://cordis.europa.eu/project/id/101008140

Appendix A. Integrals involving Chebyshev polynomials

The Chebyshev polynomial of the first and second kinds of order n are defined as:

$$T_n(t)=\cos(n\arccos t),\qquad U_n(t)=\frac{\sin[(n+1)\arccos t]}{\sin(\arccos t)}. \tag{A.1}$$

respectively, where $0\le \arccos t\le \pi$. They form a complete orthogonal set in the interval $[-1, 1]$ with respect to the weight function $(1-t)^{-1/2}$ and $(1-t)^{1/2}$, respectively, namely:

$$\int_{-1}^{1}\frac{T_n(t)T_m(t)}{\sqrt{1-t^2}}dt=\begin{cases}\pi/2, & \text{if } n=m\neq 0,\\ \pi, & \text{if } n=m=0,\\ 0, & \text{if } n\neq m.\end{cases}$$

$$\int_{-1}^{1}U_n(t)U_m(t)\sqrt{1-t^2}\,dt=\begin{cases}\pi/2, & \text{if } n=m,\\ 0, & \text{if } n\neq m.\end{cases} \tag{A.2}$$

By using the definition (A.1) and making the substitution $t=\cos\theta$, the following definite integrals can be calculated:

$$\int_{-1}^{1}\frac{U_n(\tau)}{\xi-\tau}\sqrt{1-\tau^2}d\tau=\pi\,T_{n+1}(\xi), \tag{A.3}$$

as found in Erdogan and Gupta (1972) and Gladwell (1976). Using the same substitution and the results (3.715.13) and (3.715.18) in Gradshteyn and Ryzhik (2007), also the following results can be obtained

$$\int_{-1}^{1}U_n(\tau)\sqrt{1-\tau^2}\sin[\alpha(\xi-\tau)]d\tau=\frac{\pi}{\alpha}(n+1)J_{n+1}(\alpha)\sin\left(\alpha\xi-\frac{n\pi}{2}\right), \tag{A.4}$$

$$\int_{-1}^{1}U_n(\tau)\sqrt{1-\tau^2}\cos[\alpha(\xi-\tau)]d\tau=\frac{\pi}{\alpha}(n+1)J_{n+1}(\alpha)\cos\left(\alpha\xi-\frac{n\pi}{2}\right), \tag{A.5}$$

where J_n denotes the Bessel function of the first kind of order n.

Appendix B. Calculation of definite integrals in (4.19)

Using the substitution $\tau=\cos\theta$, the definite integrals (4.19) can be calculated in closed-form:

$$C_n^{(0)}(\xi)=\int_{\arccos\xi}^{\pi/2}\sin(n+1)\theta\sin\theta\,d\theta=\begin{cases}\dfrac{\sqrt{1-\xi^2}}{2}\left[\dfrac{U_{n+1}(\xi)}{n+2}-\dfrac{U_{n-1}(\xi)}{n}\right]+\dfrac{n+1}{n(n+2)}\sin\dfrac{n\pi}{2}, & \text{for } n\neq 0,\\ \dfrac{\pi}{4}-\dfrac{\arccos\xi}{2}+\dfrac{U_1(\xi)}{4}\sqrt{1-\xi^2}, & \text{for } n=0,\end{cases} \tag{B.1}$$

$$C_n^{(1)}(\xi)=\frac{1}{2}\int_{\arccos\xi}^{\pi/2}[\cos n\theta-\cos(n+2)\theta]\cos\theta\,d\theta=\begin{cases}\dfrac{\sqrt{1-\xi^2}}{4}\left[\dfrac{U_{n+2}(\xi)}{n+3}-\dfrac{U_{n-2}(\xi)}{n-1}\right]-\dfrac{\cos(n\pi/2)}{(n-1)(n+3)}, & \text{for } n\neq 1,\\ \dfrac{\pi}{8}-\dfrac{\arccos\xi}{4}+\dfrac{U_3(\xi)}{16}\sqrt{1-\xi^2}, & \text{for } n=1,\end{cases} \tag{B.2}$$

$$C_n^{(2)}(\xi)=\frac{1}{2}\int_{\arccos\xi}^{\pi}[\cos n\theta-\cos(n+2)\theta]\cos^2\theta\,d\theta=\begin{cases}\dfrac{\sqrt{1-\xi^2}}{8}\left[\dfrac{U_{n+3}(\xi)}{n+4}+\dfrac{U_{n+1}(\xi)}{n+2}-\dfrac{U_{n-1}(\xi)}{n}-\dfrac{U_{n-3}(\xi)}{n-2}\right]-\dfrac{2(n+1)\sin(n\pi/2)}{n(n^2-4)(n+4)}, & \text{for } n\neq 0,\ 2,\\ \dfrac{\pi}{16}-\dfrac{\arccos\xi}{8}+\dfrac{U_3(\xi)}{32}\sqrt{1-\xi^2}, & \text{for } n=0,\\ \dfrac{\pi}{16}-\dfrac{\arccos\xi}{8}+\dfrac{\sqrt{1-\xi^2}}{8}\left[\dfrac{U_5(\xi)}{6}+\dfrac{U_3(\xi)}{4}-\dfrac{U_1(\xi)}{2}\right], & \text{for } n=2.\end{cases}\tag{B.3}$$

Appendix C. Numerical calculation of infinite integrals in (5.13)

The infinite integral in (5.13) involves the product of Bessel and trigonometric function which displays highly oscillatory behavior at infinite and it has the following form and can be split into two terms

$$\int_0^{\infty}\varphi(\alpha)J_{2n+1}(\alpha)\sin\alpha\xi\,d\alpha=I_n(\xi,\alpha_0)+L_n(\xi,\alpha_0),\tag{C.1}$$

where the function φ(α) is analytic in the complex half-plane Re(α) ≥ $\alpha_0 > 0$, being α_0 a real and positive value to be defined in the following, and

$$\begin{aligned}I_n(\xi,\alpha_0)&=\int_0^{\alpha_0}\varphi(\alpha)J_{2n+1}(\alpha)\sin\alpha\xi\,d\alpha,\\ L_n(\xi,\alpha_0)&=\int_{\alpha_0}^{\infty}\varphi(\alpha)J_{2n+1}(\alpha)\sin\alpha\xi\,d\alpha.\end{aligned}\tag{C.2}$$

The integral $I_n(\xi, \alpha_0)$ can be evaluated by using standard Gauss quadrature, being defined in a bounded interval. In particular, the choice $\alpha_0 = 2n+1$ is made, since the function $J_{2n+1}(\alpha)$ has no oscillation within the real interval $0 \le \alpha \le 2n+1$. For calculating the integral $L_n(\xi, \alpha_0)$ use is made of the decomposition of a Bessel function of the first kind into the sum of two Hankel functions (Gradshteyn and Ryzhik, 2007), namely

$$J_n(\alpha)=\frac{1}{2}\left[H_n^{(1)}(\alpha)+H_n^{(2)}(\alpha)\right].\tag{C.3}$$

The Hankel functions $H_n^{(1)}(\alpha)$ and $H_n^{(2)}(\alpha)$ exhibit exponential decay as α tends to infinite in the upper and lower complex halfplane, respectively, namely

$$H_n^{(1)}(\alpha)=O\left(\alpha^{-1/2}\,e^{i(\alpha-n\pi/2-\pi/4)}\right),\quad H_n^{(2)}(\alpha)=O\left(\alpha^{-1/2}\,e^{-i(\alpha-n\pi/2-\pi/4)}\right),\tag{C.4}$$

as $|\alpha|\to\infty$. Then, according to the decomposition (C.3) the integral $L_n(\xi, \alpha_0)$ can be split as

$$L_n(\xi,\alpha_0)=\frac{1}{2}\left[\int_{\alpha_0}^{\infty}\varphi(\alpha)H_{2n+1}^{(1)}(\alpha)\sin\alpha\xi\,d\alpha+\int_{\alpha_0}^{\infty}\varphi(\alpha)H_{2n+1}^{(2)}(\alpha)\sin\alpha\xi\,d\alpha\right],\tag{C.5}$$

The contours of integration of the integrals in (C.5) can be deformed in the complex α plane into a straight path parallel to the imaginary axis defined by $\alpha=\alpha_0\pm i\,\beta$, for $0\le\beta\le R$, where the plus sign is taken for the first integral and the minus sign for the second one, and a quarter of circle of radius R centred on the real axis at $\alpha=\alpha_0$, for $R\to\infty$. Then, according to the Jordan lemma the contribution of the two circular paths is vanishing small as $R\to\infty$. The contributions of the straight paths provide instead the following convergent integral, whose argument decays exponentially as $\beta\to\infty$, according to the asymptotic behavior of the Hankel functions (C.4) and that of function $g(\alpha\lambda)$

$$L_n(\xi,\alpha_0)=\mathrm{Re}\left\{\frac{e^{i\alpha\xi}}{2}\int_0^{\infty}\left[\varphi(\alpha_0+i\beta)H_{2n+1}^{(1)}(\alpha_0+i\beta)e^{-\beta\xi}-\varphi(\alpha_0-i\beta)H_{2n+1}^{(2)}(\alpha_0-i\beta)e^{\beta\xi}\right]d\beta\right\}.$$

Appendix D. Proof of result (4.19)

Let us show that the condition

$$\int_{-a}^{a}\varphi(t)dt\int_0^{\infty}\frac{\cos[s(x-t)]}{g(s\not)}ds=0,\qquad\text{for } |x|\le a,\tag{D.1}$$

where φ(t) is an odd function, i.e. $\varphi(t) = -\varphi(-t)$, necessarily implies $\varphi(t) = 0$ for $|t| \le a$.
Indeed, by exchanging the order of integration and using the odd property of φ one has

$$\int_0^{\infty}\frac{\Phi(s)}{g(s\not)}\sin sx\,ds=0,\qquad\text{for } |x|\le a,\tag{D.2}$$

where

$$\Phi(s) = \int_{-a}^{a} \varphi(t) \sin st \, dt. \tag{D.3}$$

Inversion of the Fourier sine transform then yields $\Phi(s) = 0$ for $s \geq 0$. Now, by expanding the term sin st in power series one gets

$$\sum_{k=1}^{\infty} \frac{(-1)^k s^{2k-1}}{(2k-1)!} \int_{-a}^{a} \varphi(t)\, t^{2k-1}\, dt = 0, \quad \text{for } s \geq 0. \tag{D.4}$$

Therefore:

$$\int_{-a}^{a} \varphi(t)\, t^{2k-1}\, dt = 0, \quad \text{for } k = 1, 2, \ldots \tag{D.5}$$

Now, let us expand also $\varphi(t)$ in power series

$$\varphi(t) = \sum_{j=1}^{\infty} \varphi_j\, t^{2j-1}. \tag{D.6}$$

Then, eqn (D.5) requires

$$\sum_{j=1}^{\infty} \varphi_j \int_{-a}^{a} t^{2(j+k-1)}\, dt = 0, \quad \text{for } k = 1, 2, \ldots \tag{D.7}$$

namely

$$\sum_{j=1}^{\infty} \frac{\varphi_j\, a^{2j}}{j + k - 1/2} = 0, \quad \text{for } k = 1, 2, \ldots \tag{D.8}$$

Since eqn (D.8) must hold true for every integer $k \geq 1$, then all the coefficients φ_j must be null, for $j = 1, 2, \ldots$, and thus $\varphi(t) = 0$ for $|t| \leq a$.

References

Attar, M., Karrech, A., Regenauer-Lieb, K., 2016. Non-linear analysis of beam-like structures on unilateral foundations: a lattice spring model. Int. J. Solid Struct. 88–89, 192–214.

Briscoe, B.J., Fiori, L., Pelillo, E., 1998. Nano-indentation of polymeric surfaces. J. Phys. D Appl. Phys. 31, 2395–2405.

Casolo, S., 2006. Macroscopic modelling of structured materials: relationship between orthotropic Cosserat continuum and rigid elements. Int. J. Solid Struct. 43 (3–4), 475–496.

Chang, C.S., Shi, Q., Liao, C.L., 2003. Elastic constants for granular materials modeled as first-order strain-gradient continua. Int. J. Solid Struct. 40 (21), 5565–5582.

Dempsey, J.P., Keer, L.M., Patel, N.B., Glasser, M.L., 1984. Contact between plates and unilateral supports. J. Appl. Mech. 55, 324–328.

Dhaliwal, R.S., Singh, A., 1987. Micropolar thermoelasticity. In: Hetnarski, R.B. (Ed.), Thermal Stresses II. Elsevier Science, Amsterdam, pp. 269–328.

El-Borgi, S., Usman, S., Güler, M.A., 2014. A frictional receding contact plane problem between a functionally graded layer and a homogeneous substrate. Int. J. Solid Struct. 51 (25–26), 4462–4476.

Elmustafa, A.A., Stone, D.S., 2002. Indentation size effect in polycrystalline F.C.C. metals. Acta Mater. 50, 3641–3650.

Erdogan, F., Gupta, G.D., 1972. On the numerical solution of singular integral equations. Q. Appl. Math. 29 (4), 525–534.

Eremeyev, V.A., Skrzat, A., Stachowicz, F., 2016a. On finite element computations of contact problems in micropolar elasticity. Adv. Mater. Sci. Eng. Article ID 9675604.

Eremeyev, V.A., Skrzat, A., Vinakurava, A., 2016b. Application of the micropolar theory to the strength analysis of bioceramic materials for bone reconstruction. Strength Mater. 48 (4), 573–582.

Eremeyev, V.A., Skrzat, A., Stachowicz, F., 2017. Linear micropolar elasticity analysis of stresses in bones under static loads. Strength Mater. 49 (4), 575–585.

Eringen, A.C., 1966. Linear theory of micropolar elasticity. J. Math. Mech. 16, 909–923.

Eringen, A.C., 1968. Theory of micropolar elasticity. In: Liebowitz, H. (Ed.), Fracture, An Advanced Treatise, vol. 2. Academic Press, ISBN 9780122406027.

Eringen, A.C., 1972. Nonlocal polar elastic continua. Int. J. Eng. Sci. 10, 1–16.

Eringen, A.C., 1983. On differential equations of nonlocal elasticity and solutions of screw dislocation and surface waves. J. Appl. Phys. 54, 4703–4710.

Gallagher, A.P., 1983. Bending of a free beam on an elastic foundation. J. Appl. Mech. 50 (2), 463–465.

Gladwell, G.M.L., 1976. On some unbonded contact problems in plane elasticity theory. J. Appl. Mech. 43, 263–267.

Gourgiotis, P.A., Georgiadis, H.G., 2011. The problem of sharp notch in couple-stress elasticity. Int. J. Solid Struct. 48, 2630–2641.

Gourgiotis, P.A., Zisis, Th, 2016. Two-dimensional indentation of microstructure solids characterized by couple-stress elasticity. J. Strain Anal. Eng. Des. 51, 1–14.

Gourgiotis, P.A., Zisis, T., Baxevanakis, K.P., 2016. Analysis of the tilted flat punch in couple-stress elasticity. Int. J. Solid Struct. 85, 34–43.

Gradshteyn, I.S., Ryzhik, I.M., 2007. Table of Integrals, Series, and Products. Elsevier.

Gurtin, M.E., Murdoch, A.I., 1975. A continuum theory of elastic material surfaces. Arch. Ration. Mech. Anal. 57 (4), 291–323.

Gurtin, M.E., Murdoch, A.I., 1978. Surface stress in solids. Int. J. Solid Struct. 14 (6), 431–440.

Gurtin, M., Weissmüller, J., Larche, F., 1998. A general theory of curved deformable interfaces in solids at equilibrium. Phil. Mag. 78, 1093–1109.

Jasiuk, I., Ostoja-Starzewski, M., 1995. Planar Cosserat elasticity of materials with holes and intrusions. Appl. Mech. Rev. 48 (11), S11–S18.

Karuriya, A.N., Bhandakkar, T., 2017. Plane strain indentation on finite thickness bonded layer in couple stress elasticity. Int. J. Solid Struct. 108, 275–288.

Keer, L.M., Dundurs, J., Tsai, K.C., 1972. Problems involving a receding contact between a layer and a half space. J. Appl. Mech. 39, 1115–1120.

Koiter, W., 1964. Couple stresses in the theory of elasticity Parts I and II. Nederl. Akad. Wetensch. Proc. Ser. B. 67, 17–29.

Lakes, R.S., 1986. Experimental microelasticity of two porous solids. Int. J. Solid Struct. 22 (1), 55–63.

Lakes, R.S., 1993. Strongly Cosserat elastic lattice and foam materials for enhanced toughness. Cell. Polym. 12, 17–30.

Lam, D.C.C., Yang, F., Chong, A.C.M., Wang, J., Tong, P., 2003. Experiments and theory in strain gradient elasticity. J. Mech. Phys. Solid. 51, 1477–1508.

Li, P., Liu, T.-J., 2020. The two-dimensional adhesive contact problem in the theory of couple stress elasticity. J. Adhes. Sci. Technol. 34 (10), 1062–1082.

Liu, S., Su, W., 2009. Effective couple-stress continuum model of cellular solids and size effects analysis. Int. J. Solid Struct. 46 (14–15), 2787–2799.

Ma, Q., Clarke, D.R., 1995. Size dependent hardness of silver single crystals. J. Mater. Res. 10, 853–863.

Mindlin, R.D., 1963. Influence of couple-stresses on stress concentrations. Exp. Mech. 3, 1–7.

Mindlin, R.D., 1964. Microstructure in linear elasticity. Arch. Ration. Mech. Anal. 16, 51.

Mindlin, R.D., Tiersten, H.F., 1962. Effects of couple-stresses in linear elasticity. Arch. Ration. Mech. Anal. 11, 415–448.

Nikolov, S., Han, C.-S., Raabe, D., 2007. On the origin of size effects in small-strain elasticity of solid polymers. Int. J. Solid Struct. 44 (5), 1582–1592.

Nobili, A., 2012. Variational approach to beams resting on two-parameter tensionless elastic foundations. J. Appl. Mech. 79 (2), 021010.

Nobili, A., Volpini, V., 2021. Microstructured induced band pattern in Love wave propagation for novel nondestructive testing (NDT) procedures. Int. J. Eng. Sci. 168, 103545.

Nobili, A., Radi, E., Vellender, A., 2019. Diffraction of antiplane shear waves and stress concentration in a cracked couple stress elastic material with micro inertia. J. Mech. Phys. Solid. 124, 663–680.

Radi, E., 2007. Effects of characteristic material lengths on mode III crack propagation in couple stress elastic-plastic materials. Int. J. Plast. 23 (8), 1439–1456.
Radi, E., 2008. On the effects of the characteristic lengths in bending and torsion on Mode III crack in couple stress elasticity. Int. J. Solid Struct. 45 (10), 3033–3058.
Radi, E., 2021. A loaded beam in full frictionless contact with a couple stress elastic half-plane: effects of non-standard contact conditions. Int. J. Solid Struct. 232, 111175.
Song, H.X., Ke, L.L., Wang, Y.S., 2017. Sliding frictional contact analysis of an elastic solid with couple stresses. Int. J. Mech. Sci. 133, 804–816.
Toupin, R.A., 1962. Elastic materials with couple-stresses. Arch. Ration. Mech. Anal. 11, 385–414.
Toupin, R.A., 1964. Theories of elasticity with couple stress. Arch. Ration. Mech. Anal. 17, 85–112.
Wang, Y., Shen, H., Zhang, X., Zhang, B., Liu, J., Li, X., 2018. Semi-analytical study of microscopic two-dimensional partial slip contact problem within the framework of couple stress elasticity: cylindrical indenter. Int. J. Solid Struct. 138, 76–86.
Yang, J.F.C., Lakes, R.S., 1982. Experimental study of micropolar and couple stress elasticity in compact bone in bending. J. Biomech. 15 (2), 91–98.
Yang, Y.B., Wang, Z.L., Shi, K., Xu, H., Mo, X.Q., Wu, Y.T., 2020. Two-axle test vehicle for damage detection for railway tracks modeled as simply supported beams with elastic foundation. Eng. Struct. 219, 110908.
Yildirim, B., Yilmaz, K.B., Comez, I., Guler, M.A., 2019. Double frictional receding contact problem for an orthotropic layer loaded by normal and tangential forces. Meccanica 54 (14), 2183–2206.
Yilmaz, K.B., Comez, I., Yildirim, B., Guler, M.A., El-Borgi, S., 2018. Frictional receding contact problem for a graded bilayer system indented by a rigid punch. Int. J. Mech. Sci. 141, 127–142.
Zhang, Y., Liu, X., 2019. Response of an infinite beam resting on the tensionless Winkler foundation subjected to an axial and a transverse concentrated loads. Eur. J. Mech. Solid. 77, 103819.
Zisis, Th, Gourgiotis, P.A., Baxevanakis, K.P., Georgiadis, H.G., 2014. Some basic contact problems in couple stress elasticity. Int. J. Solid Struct. 51, 2084–2095.
Zisis, T., Gourgiotis, P.A., Dal Corso, F., 2015. A contact problem in couple stress thermoelasticity: the indentation by a hot flat punch. Int. J. Solid Struct. 63, 226–239.
Zisis, Th, Gourgiotis, P.A., Georgiadis, H.G., 2018. Contact mechanics in the framework of couple stress elasticity. In: Altenbach, H., et al. (Eds.), Generalized Models and Non-classical Approaches in Complex Materials 2, Advanced Structured Materials, vol. 90. Springer, pp. 279–306 (Chapter 14).